Few-Femtosecond Isotope Effect in Polyatomic Molecules Ionized by Extreme Ultraviolet Attosecond Pulse Trains

Morgane Vacher, Alexie Boyer, Vincent Loriot, Franck Lépine, Saikat Nandi

Few-femtosecond isotope effect in polyatomic molecules ionized by extreme ultraviolet attosecond pulse trains

Morgane Vacher,*,† Alexie Boyer,‡ Vincent Loriot,‡ Franck Lépine,‡ and Saikat Nandi*,‡

†*Nantes Université, CNRS, CEISAM UMR 6230, F-44300 Nantes, France*

‡*Université de Lyon, Université Claude Bernard Lyon 1, CNRS, Institut Lumière Matière, F-69622 Villeurbanne, France*

E-mail: morgane.vacher@univ-nantes.fr; saikat.nandi@univ-lyon1.fr

Abstract

Following ionization by an extreme ultraviolet (XUV) attosecond pulse train, a polyatomic molecule can be promoted to more-than-one excited states of the residual ion. The ensuing relaxation dynamics is often facilitated by several reaction coordinates, making them difficult to disentangle by usual spectroscopic means. Here, we show that in atto-chemistry isotope labelling can be an efficient tool for unraveling the relaxation pathways in highly excited photo-ionized molecules. Employing a XUV pump pulse and a near-infrared probe pulse, we found the nuclear as well as coupled electron-nuclear dynamics in ethylene to be almost 40% faster compared to its deuterated counter-part. The findings, which are supported by advanced non-adiabatic dynamics calculations, led to the identification of the relevant nuclear coordinates controlling the relaxation. Our experiment highlights the relevance of ultrashort XUV pulses to capture the isotopic effect in few-femtosecond molecular photo-dynamics.

Introduction

Following pioneering works of A. H. Zewail,[1] femto-chemistry experiments have provided many important insights about light-induced dynamics in complex molecules. These experiments usually involve studying the relaxation of a particular electronic state in the neutral molecule, excited resonantly via ultraviolet or, visible laser pulses. With the advent of high-order harmonic generation (HHG) based tabletop sources providing attosecond and few-femtosecond pulses in the extreme ultraviolet (XUV) domain, it is now possible to investigate ultrafast relaxation processes in photo-ionized systems, leading to the development of atto-chemistry.[2–4] Ionization by an ultrashort XUV pulse, spanning several electron-volts results in emission of an electron from the valence as well as inner-valence levels leaving behind highly excited species, where probing out-of-equilibrium electron and nuclear dynamics are of great interests. Notable examples include electron localization in hydrogen molecule,[5] charge migration in amino acids,[6] coupled electron-nuclear dynamics,[7] and relaxation of correla-

tion bands[8] in polycyclic aromatic hydrocarbons, and hydrated electron formation in water clusters,[9] just to name a few. Contrary to femto-chemistry experiments, photoionization of a molecule by a broadband XUV pulse is accompanied by excitation of several of its cationic states at the same time, leading to relaxation dynamics that involves different pathways facilitated by different nuclear coordinates. This poses a unique challenge in atto-chemistry experiments: how to disentangle the relaxation pathways undertaken simultaneously by the molecular cation and associate them with a relevant coordinate?

Here, we show that by comparing the relaxation timescales between two isotopologues, ethylene (C_2H_4) and its deuterated counterpart (C_2D_4), one can determine the nuclear coordinates that govern the underlying reaction pathways in the XUV-ionized species. Compared to C_2H_4, the change in zero-point energy is about 15 meV in C_2D_4.[10] Despite such a tiny change of 0.1%, we found that both nuclear and coupled electron-nuclear dynamics in C_2H_4 could be faster by as much as 40% compared to C_2D_4. Furthermore, we were able to measure isotope effects on a timescale as short as $5 - 10$ fs between the two isotopologues. These observations are in excellent agreements with theoretical results obtained from non-adiabatic semi-classical dynamics simulations based on multi-reference electronic structure calculations.

The article is structured as follows: In the next section, the concept of the experiment is exposed. Then, the experimental and theoretical methods used are presented, including details of the data analysis. In the subsequent section, the results are presented and discussed. The last section offers some concluding remarks.

Scientific Premise

Being the simplest alkene in nature, ethylene served as a test-bench in several experiments involving resonant excitation by ultraviolet pulses.[11–14] Pioneering efforts to study XUV-induced fragmentation dynamics in ethylene began more than a decade ago,[15] with Ludwig

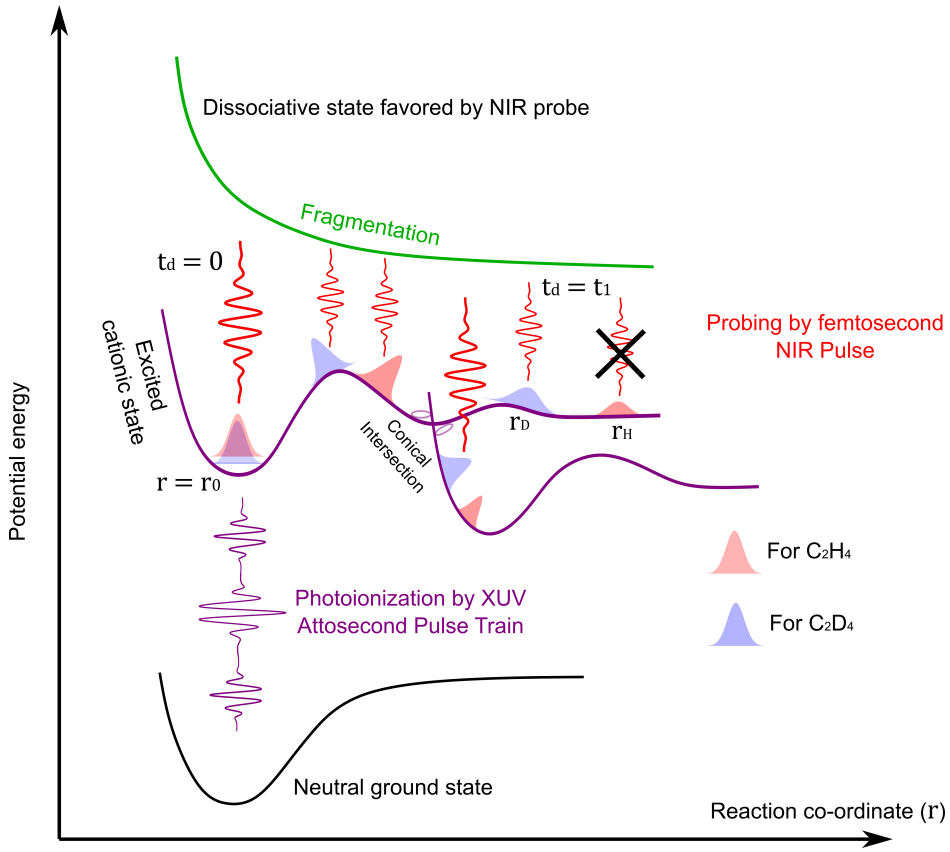

Figure 1: Pump-probe scheme for studying isotope effect. Both molecules were ionized from their neutral ground states by an XUV-APT. At pump-probe delay, $t_d = 0$ a nuclear wave-packet (red) is launched at a position $r = r_0$ in the potential energy surface of an excited state in $C_2H_4^+$. It explores the potential energy surface and reaches a relaxed configuration: $r = r_H$ (at $t_d = t_1$), from where excitation to the dissociative state is no longer favored by the NIR probe. In case of $C_2D_4^+$, due to the isotopic substitution the corresponding nuclear wave-packet (blue) reaches a different point ($r = r_D$) in the potential energy surface at $t_d = t_1$. From there, the NIR probe can still promote the wave-packet to the dissociative state. Thus, the decay rate becomes different in the two systems.

et al. carrying out more recent investigations containing improved temporal resolution.[16] In our experiment, after ionizing C_2H_4 and C_2D_4 by a XUV attosecond pulse train (APT), we monitored the ensuing relaxation dynamics in the molecular cation using a near infrared (NIR) pulse. After photoionization by the XUV-pump (photon energy: $17 - 23.5$ eV, well below the photo-double ionization threshold of ethylene), a nuclear wave-packet is launched into the excited states of $C_2H_4^+$ (see Fig. 1, the 'red' wave-packet). In contrast to femto-chemistry experiments, where only one electronic state is excited, here the pump

pulse populates the ground cationic state Ex0 ($X\ ^2B_{3u}$) as well as three excited cationic states: Ex1 ($A\ ^2B_{3g}$), Ex2 ($B\ ^2A_g$), and Ex3 ($C\ ^2B_{2u}$) (see Fig. S1 in the Supporting Information). The population in these excited states can decay to a low-lying level through a conical intersection[17] via coupled electron-nuclear motion, or relax via nuclear dynamics such as bond-dissociation, structural rearrangement. When the pump and probe pulses are synchronized in time ($t_d = 0$) and the reaction co-ordinate ($r = r_0$) is same as the neutral geometry at equilibrium, the probe depopulates the excited state by promoting part of its population to a higher lying dissociative state leading to production of ionic fragments. If the probe arrives at a delay $t_d = t_1$ after the pump, the reaction coordinate is $r = r_H$, the wave-packet has evolved and the population has relaxed through any of the above mechanisms. Hence, the NIR pulse can no longer efficiently promote the nuclear wave-packet to the dissociative state and the probability for producing the relevant fragment decreases, causing exponential decay in the measured photo-ion yield as a function of the pump-probe delay. For $C_2D_4^+$, due to increase in mass the nuclear wave-packet can reach a different value of the reaction coordinate: $r = r_D$ in the potential energy landscape at $t_d = t_1$ (see Fig. 1). This means that the population can remain on the potential energy surface of the excited state for longer time than $C_2H_4^+$, eventually permitting the NIR probe to promote the wave-packet to the dissociative state over a longer time, leading to a slower decay. It is worth noting that the timescale of a particular fragment ion in the two-color signal is primarily dependent on the underlying relaxation process. While it is possible to obtain the same timescale for several fragments from a given system,[18] here, we found the timescales to vary significantly depending on the fragment, indicating that they are in fact governed by different nuclear degrees of freedom. In the following, we therefore highlight three different relaxation pathways by choosing three different fragments, H^+, H_2^+ and CH_2^+ as well as their corresponding isotopologues.

Methods

In this section, the experimental and theoretical methods used in the present work are presented. First, the eperimental setup is described. Then, the data analysis of the measurements is detailed. Last, the theoretical electronic structure and dynamics methods, as well as computational details, are presented.

Experimental methods

The experiments were performed using a commercial Ti-Sapphire laser system (Legend USX) providing femtosecond NIR (central wavelength: 805 nm) pulses (energy: 2 mJ) at 5 kHz repetition rate. The amplifier output was split in two equal parts using a beam-splitter along the two arms of a Mach-Zehnder interferometer. One part ('pump' arm) was used to produce the XUV radiation via high-order harmonic generation in Krypton. The co-propagating NIR beam was filtered out using an Nb_2O_5 beam-splitter followed by a 200 nm thick Sn-filter. The resulting XUV spectra, containing three odd-order high-harmonics from 11^{th} to 15^{th} (see Fig. S1 in the Supporting Information) was focused unto the target gas using a gold-coated toroidal mirror. The NIR beam on the 'probe' arm was focused using a lens having focal length of 1 m. The pump and probe pulses were recombined via a drilled mirror. The use of a refractive delay-line unit consisting of a pair of wedges allowed us to cover a wide range of delay (from -180 fs to $+400$ fs) between the arrivals of the two pulses, without introducing a significant change on the pulse duration (< 1 fs) due to the dispersion. Here, negative delays implied that the probe arrived before the pump and vice versa. The target molecules were introduced as an effusive jet in the interaction region of a velocity map imaging spectrometer operating in the ion time-of-flight mode. The target number density was estimated to be around $5 \times 10^{11}/\text{cm}^3$. The peak intensity of the NIR probe pulse at the focus was varied between $4 - 9$ TW/cm^2. The duration (FWHM) of the NIR pulse was found to be 26 ± 1 fs (see Fig. S2 in the Supporting Information). The cross-correlation between the XUV pump

and the NIR probe, measured using photoionization of argon, was found to be 36 ± 4 fs, indicating a duration (FWHM) of $24 - 30$ fs for the XUV pulse. Ethylene (purity>99%) and deuterated ethylene (95%) were purchased from Sigma-Aldrich and used without further purification.

Data analysis

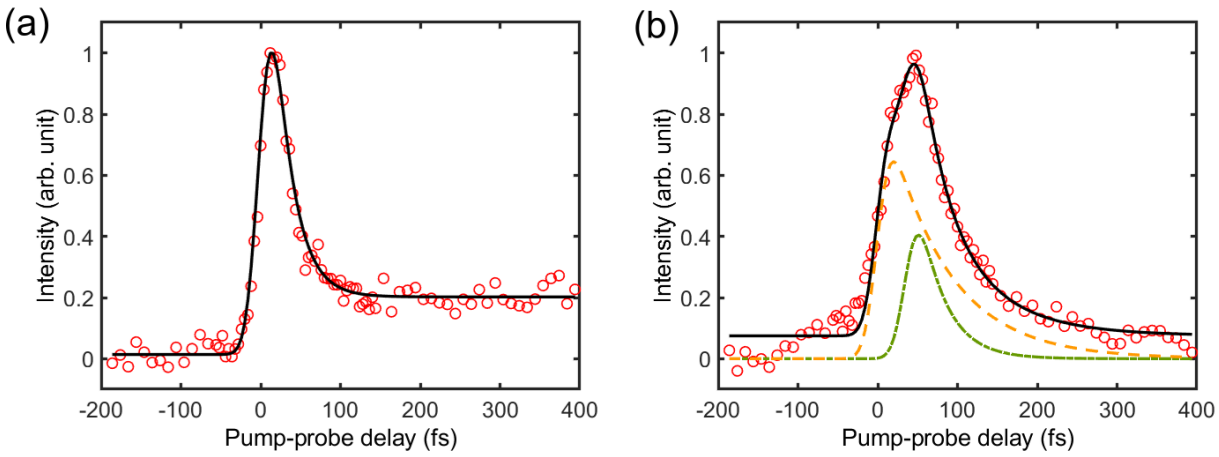

Figure 2: (a) Experimental transient signal for H^+ ion, as a function of the pump-probe delay. Open circle: experimental data; solid line: fit with $f(t)$. (b) Same as (a), but for CH_2^+ fragment. Note that in this case two exponential decay functions are required to fit the experimental data correctly. Open circle: signal from experiment; solid line: fit with $g(t)$; dashed line: decay with τ_{slow}; dashed-dotted line: decay with τ_{fast}.

The XUV-only signal for a given fragment has been subtracted at each delay point from the corresponding two-color signal (XUV+NIR). Afterwards, the timescale was extracted by fitting this difference signal with an exponential decay function convoluted with a normalized Gaussian function representing the instrument response. See Fig. 2(a) for typical pump-probe delay-dependent H^+ yield at 9 TW/cm^2 NIR-intensity (open circles) and the corresponding fit (solid line). The complete fitting function can be expressed as: $f(t) = \left[\{A \exp\left(-\frac{t-t_0}{\tau}\right) + B\}\Theta\left(t - t_0\right)\right] * f_{\text{IRF}}\left(t\right) + C$. Here, $f_{\text{IRF}}\left(t\right)$ is the instrument response function, given by: $f_{\text{IRF}}\left(t\right) = \frac{1}{\sigma\sqrt{2\pi}} \exp\left[-\left(\frac{t}{\sigma\sqrt{2}}\right)^2\right]$. τ is the time constant for the exponential decay, t_0 denotes the temporal overlap between the two pulses, σ is the vari-

ance associated with $f_{\mathrm{IRF}}(t)$ and $\Theta(t-t_0)$ denotes a Heaviside step function. The term C corresponds to a linear background, subtracted from the transient signal at each probe intensity. After fitting the transient signal with $f(t)$, we have determined the signal-to-noise ratio (SNR) by taking the root-mean-square of the residue (difference between the measured signal and the fit) at each delay point. The SNR was found to be 28. It is used as an input for the Monte-Carlo simulation as described in previous works,[8] to determine the accuracy of the extracted time-constants for a fixed value of σ. As shown in Fig. S3 in the Supporting Information, the timescales can be accurately extracted down to 10 fs. Fig. 2(b) shows the transient signal for the CH_2^+ fragment as a function of pump-probe delay at 9 TW/cm^2 NIR intensity. Two exponential decay functions with unequal time-constants are required to fit the ion yield. To fit the transient signal for CH_2^+ using two exponential decays, the function was changed to: $g(t) = \left[A\,\exp\left(-\frac{t-t_0}{\tau_{\mathrm{slow}}}\right)\Theta(t-t_0) + B\,\exp\left(-\frac{t-t_0}{\tau_{\mathrm{fast}}}\right)\Theta(t-t_0-\Delta t)\right] * f_{\mathrm{IRF}}(t) + C$. Here, Δt denotes the time lag between the two decay functions with two different decay constants, $\tau_{\mathrm{slow}} > \tau_{\mathrm{fast}}$. The faster decay ($\tau_{\mathrm{fast}}$; dashed-dotted curve) is lagging behind the slower one (τ_{slow}; dashed curve) by Δt. Each τ-value was obtained from the difference signal cumulatively averaged over twenty consecutive scans across the entire temporal window of -180 fs to $+400$ fs. We used the Levenberg-Marquardt algorithm for fitting the difference signal. The uncertainties reported here represent the errors obtained from this fitting procedure only. These errors were further used to obtain the weighted average of the measured time constants at different probe intensities for a particular fragment. For N time-constants τ_1, τ_2, ... τ_N with N corresponding uncertainties δ_1, δ_2, ... δ_N, obtained at N different probe intensities, the weighted average is given by, $\bar{\tau} = \frac{\sum_{i=1}^{N} w_i \tau_i}{\sum_{i=1}^{N} w_i}$, where $w_i = 1/\delta_i^2$ is the weight. The uncertainty on the weighted average can be expressed as, $\bar{\delta} = \sqrt{\frac{N\sum_{i=1}^{N} w_i(\tau_i-\bar{\tau})^2}{(N-1)\sum_{i=1}^{N} w_i}}$.[19] Finally, the 95% confidence interval can be designated as: $\bar{\tau} \pm \frac{1.96\,\bar{\delta}}{\sqrt{N}}$. To maintain consistency in the fitting procedure, the values for σ and t_0 have been assumed to be the same in case of all the fragments for a given target molecule at a given NIR intensity. The value of the parameter $2\sigma\sqrt{2ln2}$ in different cases was found to vary from $26-32$ fs, which is reasonably

close to the measured cross-correlation. Similarly, the values for t_0 were found to be within -3 to 6 fs in various cases, which is rather close to the step size (4 fs) used for the temporal scan.

Theoretical methods

The electronic structure of both isotopic molecules was studied using the complete active space self-consistent field (CASSCF) method,[20] equally averaged over the first five doublet states: Ex0, Ex1, Ex2, Ex3 and Ex4. In all molecules, the active space used consisted of 11 electrons distributed in 12 orbitals: the four σ and four σ^* orbitals of the four C-H bonds, the σ and four σ^* orbitals of the C=C bond, and the π and π^* orbitals of the C=C bond (see Fig. S4 in the Supporting Information). It is noted that all valence electrons are active. Only the core 1s electrons of the carbon atoms are inactive. This allows, in principle, for any chemical bond to break or form. The ANO-RCC basis set with polarized double-zeta contraction (ANO-RCC-VDZP)[21] and the atomic compact Cholesky decomposition (acCD)[22] were used.

Non-adiabatic "on-the-fly" dynamics were simulated using the trajectory surface hopping method with Tully's fewest switches algorithm.[23] The nuclear motion was treated classically by numerically integrating Newton's equations of motion using the velocity Verlet algorithm. A time step of 20 a.u., i.e. about 0.48 fs was used. All nuclear coordinates were taken into account. Non-adiabatic transitions among any of the five lowest-energy doublet states were included. The decoherence correction suggested by Granucci and Persico was used with a decay factor of 0.1 hartree.[24] The implementation of the above methods in the OpenMolcas (version *19.11-586-g8ab414a*) package[25] was used.

For each molecular system, 100 trajectories were initiated on either Ex1, Ex2 or Ex3 state, around the equilibrium structure of the electronic ground state of the neutral species. Both initial positions and momenta were sampled from a Wigner distribution[26] to mimic the vibrational ground state before photoionization; this was performed using the Newton-X

package.[27]

The absolute values of the nuclear coordinates as a function of time were calculated as a mean over the different bond lengths (or, angles) in the molecule allowing for better statistics. These absolute values for different coordinates oscillate rapidly as a function of time (see Fig. S5 in the Supporting Information). Thus, the variations of the nuclear coordinates, reported below, were obtained by performing a moving average of the corresponding absolute values over a time-window. The duration of the time-window for the moving average was chosen to be significantly longer than the period of oscillations for all these coordinates. The period of C–H stretching, C=C stretching and H–C–C bending being typically $20-25$ fs, we used a fixed time-window of 50 fs for performing the moving average and extracted only the corresponding trend as a function of time for the purpose of comparing with the experimental τ-values. By choosing 50 fs as the averaging window for all the fragments, we could effectively remove the fast oscillating behavior of all the co-ordinates as a function of time, allowing us to compare quantitatively the experimental isotope effect with the theoretical ones. An even wider time-window would lead to mixing of the trends at shorter timescale with those at longer timescales, to which the NIR probe was not sensitive.

Results and Discussions

In this section, the measured fragmentation dynamics are presented and discussed in light of the simulations. More precisely, the H^+ (D^+), H_2^+ (D_2^+) and CH_2^+ (CD_2^+) fragment dynamics are interpreted in terms of different relaxation pathways occurring upon XUV photoionization: dissociation, structural rearrangements and non-adiabatic transitions, respectively.

Relaxation via dissociation

The relaxation dynamics with the shortest time-scale was measured for the H^+ ions. The transient signal (difference between the XUV+NIR and XUV-only signals) as a function of

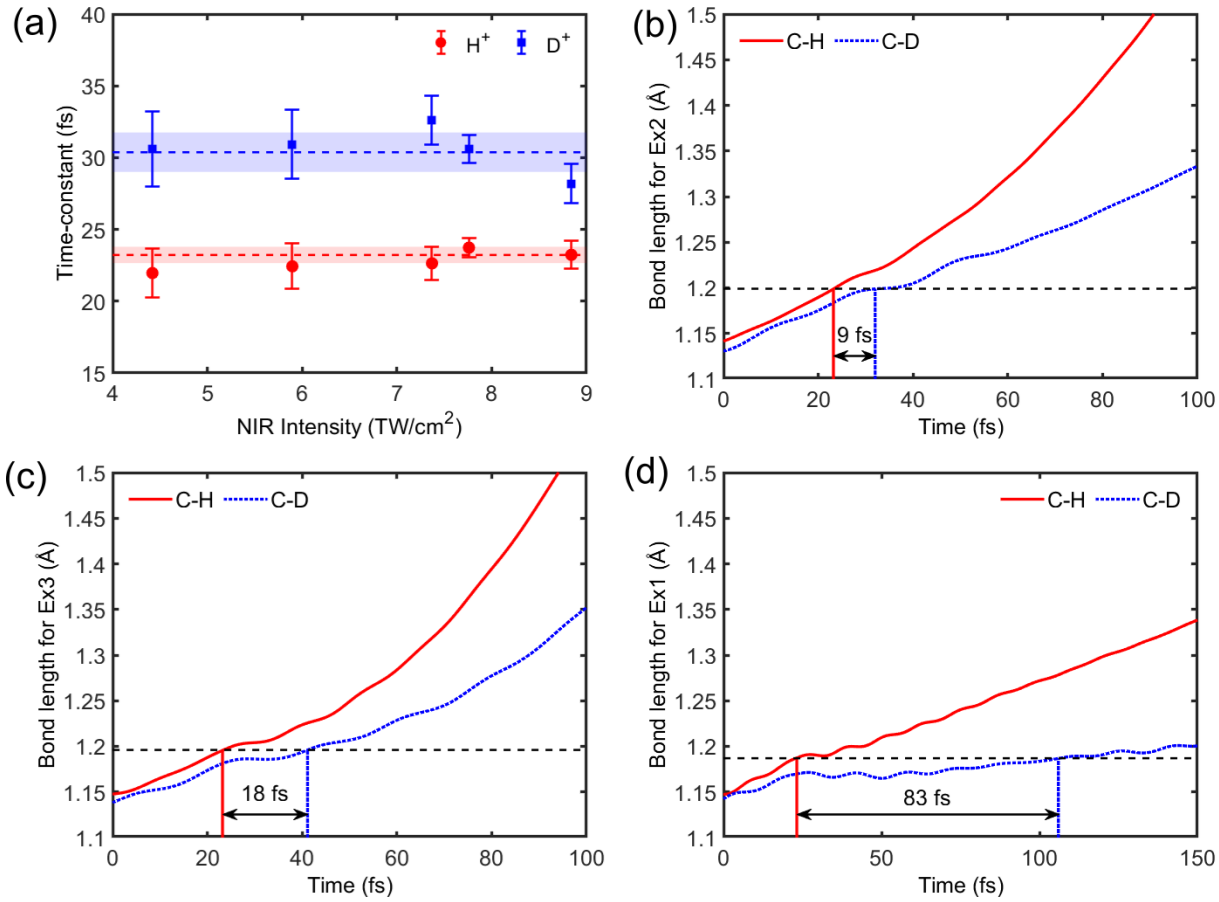

Figure 3: (a) Solid circles (squares): time-constants obtained for the H^+ (D^+) fragments at different NIR intensities. The dashed line in each case corresponds to the weighted average and the shaded area represents the 95% confidence interval. (b) Average temporal variation of the C–H (red curve) and C–D (blue dotted curve) bond-length for Ex2 state. The averaging was performed using the procedure described in the Theoretical Methods. (c) and (d) Same as (b), but for Ex3 and Ex1 state, respectively.

the pump-probe delay was fitted with an exponential decay function convoluted with the instrument response function to extract the experimental time-constants, τ (see Supporting Information for details about the fitting procedure). The τ-values for H^+ and D^+ at different probe intensities are shown in Fig. 3(a). The τ-values for both molecules do not change as a function of the NIR-probe intensity, allowing us to consider only the XUV-induced dynamics in the cation. The reason behind the extracted timescales being independent on the NIR probe intensity can be attributed to the fact that the main role of the probe is simply to deplete the population in the excited state (see Fig. 1). The timescales are representative

of the dynamics initiated by the XUV-pump only. If the probe is too weak, it is unable to transfer the population to the dissociative state, which reduces the subsequent production of the ionic fragments but it could not affect the relaxation time inherent to the population in the excited state. On average, $\tau_{H^+} = 23.2 \pm 0.6$ fs is faster by 7 ± 2 fs compared to $\tau_{D^+} = 30.4 \pm 1.4$ fs. We propose the formation of H^+ (or, D^+) ions in the two-color signal to stem from the dominant reaction channel involving loss of an H-atom in the photo-excited cation.[28] Indeed, as shown in Fig. 3(b), for both molecules the corresponding trend in bond-length for Ex2 state increases rapidly with time, denoting bond-dissociation. It should be noted that significant number of dissociation events were observed in the dynamical evolution of these two bonds, in contrast to previous theoretical studies.[16,29] This could be attributed to the use of a multi-reference electronic structure method together with a large active space. In addition, the rate of increase in C–D is slower than that in C–H bond: the heavier D-atom takes longer to reach the same distance compared to the lighter H-atom. Within $\tau_{H^+} = 23.2$ fs, the C–H bond elongates to 1.2 Å (the red vertical line). To reach the same value (see the horizontal dashed line), the C–D bond takes 32 fs (the blue vertical line). The difference of almost 9 fs matches quantitatively with the isotope effect of 7 ± 2 fs in the τ-values, supporting our assumption that indeed the decay in H^+ or, D^+ ions are signatures of the relaxation process mediated by the C–H or, C–D dissociation. Similarly, inspecting the evolution of these two bonds in the Ex3 state (see Fig. 3(c)), we found the corresponding difference in time to be almost 18 fs that matches only qualitatively with the observed isotope effect, implying that although Ex2 plays the dominant role, Ex3 can also contribute to the underlying relaxation process. However, for the Ex1 state, we noticed an isotope effect that is an order of magnitude higher than the experimental value (see Fig. 3(d)). All of these enable us to identify Ex2 as the most relevant electronic state where the relaxation process takes place.

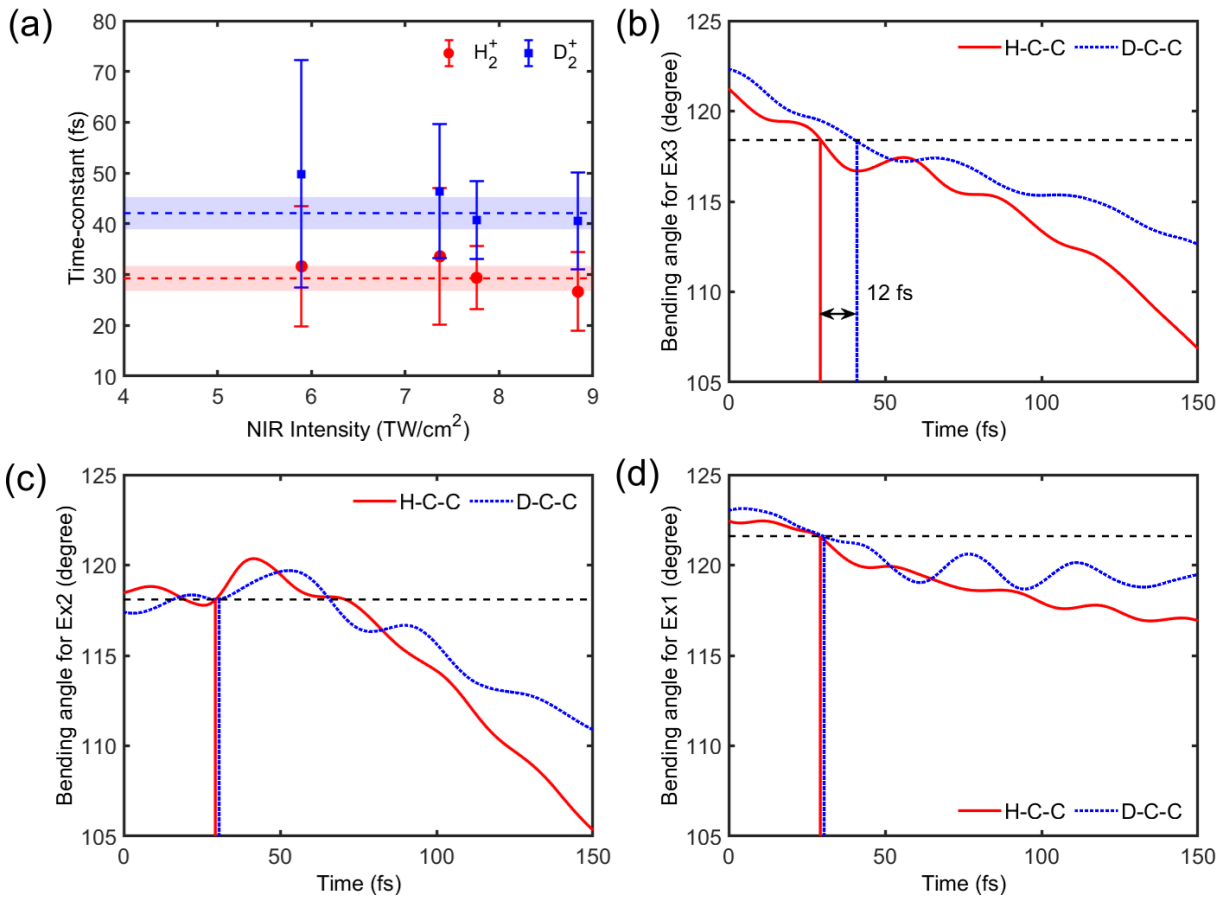

Figure 4: (a) Solid circles (squares): experimental time-constants for H_2^+ (D_2^+) at different intensities of the NIR probe. As before, the dashed lines denote weighted average for the respective time-constant, whereas the shaded area signifies 95% confidence interval. (b) The time-dependent average variation of the H–C–C (red curve) and D–C–C (blue dotted curve) angles for excitation to the Ex3 state. The same for (c) the Ex2 state and (d) the Ex1 state are also shown.

Relaxation via structural rearrangements

Additional changes in the molecular geometry, such as structural rearrangement can also initiate relaxation processes in the ethylene cation. To understand better its role in the relaxation dynamics, we studied the time-dependent formation of H_2^+ ion. The corresponding τ-values as a function of the NIR probe intensity for both H_2^+ and D_2+ are shown in Fig. 4(a). Once again, the average value for $\tau_{H_2^+} = 29.3 \pm 2.5$ fs is smaller compared to that of $\tau_{D_2^+} = 42.1 \pm 3.2$ fs. Despite overlapping error-bars, the 95% confidence intervals do not overlap, thus allowing us to extract an isotope effect of 13 ± 6 fs. The values of $\tau_{H_2^+}$

are significantly (26%) higher than τ_{H^+} indicating a relaxation pathway possibly different from the C–H bond-dissociation. We propose this pathway to be facilitated by the H–C–C bending coordinate that brings two hydrogen atoms closer compared to the neutral geometry. A related mechanism had been proposed previously in connection with H_2^+ formation from ethylene cation.[15] We carried out an identical analysis as before for the average variations in H–C–C and D–C–C angles as a function of time. As shown in Fig. 4(b) for the Ex3 state, the trends in both angles reduce rapidly indicating movement of a hydrogen atom from one of the carbon atoms to the other. During the time interval $\tau_{H_2^+} = 29.3$ fs, the H–C–C angle reduces to 118.4° (marked by the red vertical line). The D–C–C angle reaches the same value (dashed horizontal line) almost 12 fs later (see the blue vertical line). The difference in time agrees quantitatively with the experimental isotope effect mentioned above. For excitation to both Ex2 and Ex1 states, no noticeable isotope effect during the time interval comparable to $\tau_{H_2^+}$ or, $\tau_{D_2^+}$ can be found (see Fig. 4(c) and (d), respectively). The difference in initial values of the angles for different electronic states in a molecular cation can be attributed to the averaging of their corresponding absolute values, as explained in Theoretical methods. Clearly, Ex3 is the main electronic state from which the NIR probe transfers the population to the dissociative state. However, the large uncertainties for the individual τ-values (see Fig. 4(a)) also indicate that only a small population on Ex3 decays via this H–C–C (or, D–C–C) bending angle leading to a low probability of formation for H_2^+ or, D_2^+. This, in turn, implies the possible existence of competing pathways for the population to undergo relaxation from the Ex3 state on a timescale faster than the dynamics facilitated by this particular coordinate.

Relaxation via non-adiabatic transition

Apart from the nuclear dynamics associated with the C-H moiety, distortions along the C=C bond can also drive relaxation processes in the photo-excited $C_2H_4^+$. Indeed, according an analysis of the initial and hopping geometries in the theoretical simulations, the most

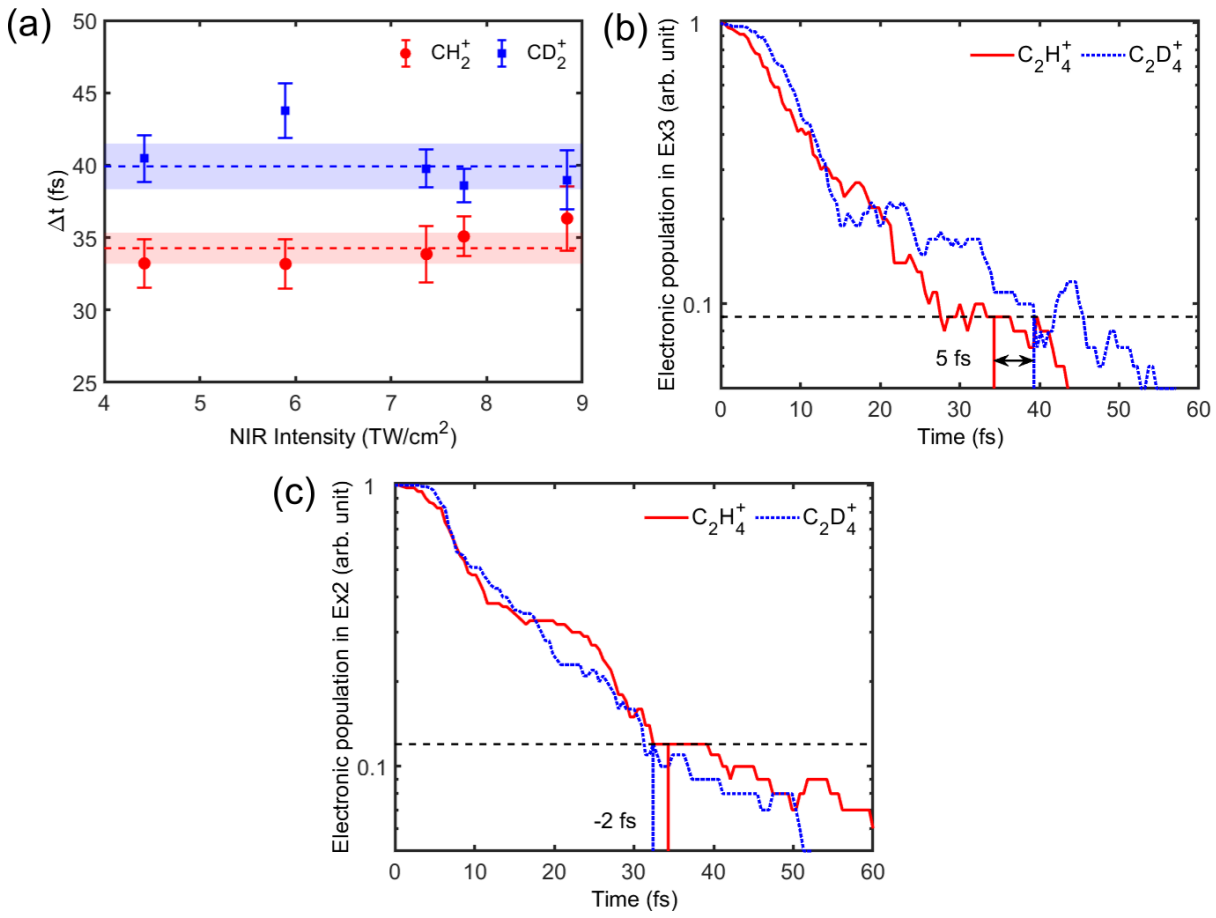

Figure 5: (a) The values of Δt as a function of the NIR probe intensity for both the molecules, along with their respective averages (dashed lines) and 95% confidence intervals (shaded areas). (b) Decay of the electronic population from the Ex3 state (red solid line) and $C_2D_4^+$ (blue dashed-dotted line). (c) The same as (b), but from the Ex2 state.

important coordinate that induces the non-adiabatic relaxation from Ex1 to Ex0 is the change of C=C bond-length. To shed light on the role of this coordinate, we investigated the decay associated with the CH_2^+ photo-ion, produced via symmetric dissociation of the C=C bond. Although the yield of CH_2^+ can overlap with that from $C_2H_4^{++}$, the doubly charged ion is metastable with long lifetime[30] and hence, could not contribute to the time-dependent signal for CH_2^+. As already shown in Fig. 2(b), for CH_2^+, we required two decay functions with unequal time-constants, separated by a time lag (Δt) to fit the experimental transient signal. It can be understood as follows: the nuclear wave-packet launched in the excited cationic state splits in two parts at $t_d \approx 0$. One part remains in the same potential energy

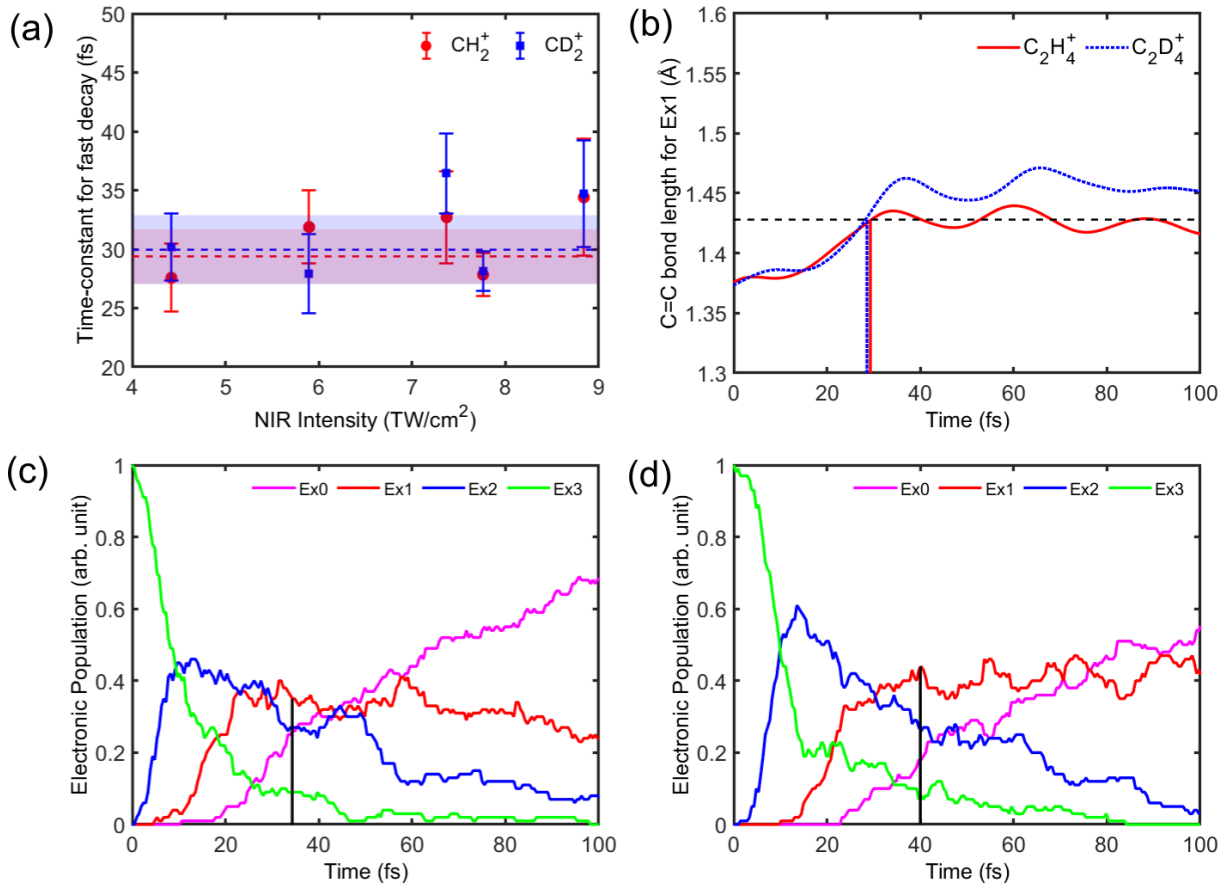

Figure 6: (a) Time constants for the fast decay (τ_{fast}) shifted by Δt, as observed in case of CH_2^+ (solid red circles) and, CD_2^+ (solid blue squares). The weighted averages (dashed lines) for τ_{fast} and 95% confidence intervals (shaded areas) are also shown. (b) The average variation of the C=C bond-length as a function of time for $C_2H_4^+$ (solid red curve) and $C_2D_4^+$ (blue dotted curve). (c) Decay of the electronic population in $C_2H_4^+$ for excitation to the Ex3 state. After $\Delta t = 34.3$ fs (denoted by black vertical line) the electronic state containing maximum of the electronic population is the Ex1 state (red curve). (d) Same as (c), but in $C_2D_4^+$. Once again, the maximum probability of finding the system after $\Delta t = 40$ fs (black vertical line) is the Ex1 state.

surface, whereas the other part transits to a lower excited state via a conical intersection, before undergoing further nuclear relaxation. Δt can be interpreted as the time for this non-adiabatic transition to take place. The two exponential decays correspond to the relaxation processes in the two different electronic states. The values of Δt as a function of NIR probe intensity is shown in Fig. 5(a). For $C_2H_4^+$, we obtained an average value of $\Delta t = 34.3 \pm 1.2$ fs which is almost 6 ± 2 fs faster than the average value of $\Delta t = 40 \pm 2$ fs in $C_2D_4^+$. Even though

the potential energy surfaces do not change due to isotopic substitution, the velocity with which the nuclear wave-packet approaches the conical intersection changes due to change in mass and hence, the time for non-adiabatic relaxation as well. Furthermore, if most of the population is transferred from Ex1 to Ex0 within the first few femtoseconds,[16,31] we could not have observed the exponential decay following Δt. Hence, the non-adiabatic relaxation can occur only from Ex3 or, Ex2. The decay of the electronic population from Ex3 state, as obtained from theoretical calculations, is shown in Fig. 5(b). To enhance the isotope effect in the region of interest we have plotted the population in log-scale. From here, we could see that after 34.3 fs, the population level reduces to almost 9% for $C_2H_4^+$ (see the red vertical line). To reach the same level (dashed horizontal line), $C_2D_4^+$ takes longer time, around 39.3 fs (see blue vertical line). Once again, the time difference of 5 fs matches quantitatively with the experimental isotope effect. Interestingly, for Ex2, the rate of decay of the population is slightly faster in $C_2D_4^+$ compared to $C_2H_4^+$: to reach the same level of 12% the former takes about 2 fs less than the latter (see Fig. 5(c)). Combining both cases, we can clearly infer that the measured Δt-values represent the non-adiabatic transition from the Ex3 state, rather than from Ex2 state. For the fast decay process following Δt, we show the relevant time-constants as a function of the NIR probe intensity in Fig. 6(a). No significant difference in the average experimental τ-values (29.4 ± 2.6 fs for CH_2^+ and 30 ± 3.3 fs for CD_2^+) can be found. For both molecules, the most probable state in which the nuclear wave packet can be found after Δt is the Ex1 state (see Fig. 6(c) and (d)). Indeed, as shown in Fig. 6(b) the average variation of the C=C bond length in Ex1 state is near identical for both isotopologues (see the vertical lines) during the first 30 fs. This suggests that after reaching the Ex1 state the population relaxes even more via stretching of the C=C bond. The time-constants of the slower decay in both molecules show clear dependency on the intensity of the NIR probe, making the relevant isotope effect difficult to observe unambiguously (see Fig. S6 in the Supporting Information). In addition, the absolute values are larger for τ_{slow}, close to 100 fs, hinting towards a different relaxation mechanism in this case.

Conclusions

In conclusion, we have shown that time-resolved mass spectrometry using ultrashort XUV and NIR pulses can distinguish the relaxation time-scales that differ from each other by only a few femtoseconds between two isotopologues. The kinetic isotope effect due to isotopic substitution is well known, as can be seen from many femto-chemistry experiments[32–34] as well as with growing interests of studying it in the context of atto-chemistry.[35–37] Here, we could establish that the observed and simulated isotope effect can in fact be used to identify the relevant electronic states and nuclear coordinates involved in the relaxation processes, resulting from the simultaneous ionization and excitation of several cationic states in the molecule by the XUV attosecond pulse train. The timescale extracted here provides an indirect measure to the relaxation process initiated by only the XUV-pump. While it does not exclude the involvement of other coordinates in XUV-induced photoionization of ethylene, our approach provides a way to identify the dominant nuclear coordinates along with the electronic states. The technique is introduced for laboratory-based HHG sources, but it is equally applicable to similar experiments being developed at free-electron laser facilities.[38] In there, of particular interests is the ultrashort X-ray pulses as pump to study relaxation processes following core-ionization.[39] However, as a molecule becomes more complex structurally, it becomes even more difficult to determine precisely the relevant reaction coordinate, especially with several cationic states excited at the same time, by comparing time-resolved measurements with quantum chemistry calculations. The universal character of isotope labelling as a tool to investigate the relaxation pathways, especially for non-adiabatic transitions could be extremely effective in these situations. The results obtained here for ethylene paves the path for such experiments at the crossroad of attoscience and molecular photo-physics and chemistry.

Author Information

Corresponding Authors

*(M.V.) E-mail: morgane.vacher@univ-nantes.fr.

*(S.N.) E-mail: saikat.nandi@univ-lyon1.fr.

Author Contributions

S.N. conceived and led the project. A.B., V.L., F.L., and S.N. carried out the experiments. V.L. developed the codes for data acquisition and data analysis. S.N. analyzed the data. M.V. performed the theoretical calculations. M.V., A.B., S.N., and F.L. interpreted the results. S.N. wrote the manuscript with inputs from all the authors.

Notes

The authors declare no competing financial interest.

Acknowledgement

We thank CNRS, Fédération de Recherche André Marie Ampère (FRAMA) and Agence Nationale de la Recherche (ANR Circé, ANR-16-CE30-0012) and COST ATTOCHEM for financial support. M. V. further acknowledges for financial support the EUR LUMOMAT project and the Investments for the Future program ANR-18-EURE-0012. The simulations were performed using HPC resources from GENCI – IDRIS (Grants 101124 and 101353) and CCIPL (Le centre de calcul intensif des Pays de la Loire).

Supporting Information Available

Measured spectral profile of XUV-pump and temporal profile of NIR-probe; Monte-Carlo simulation on how to extract timescale shorter than cross-correlation; calculated active orbitals in ethylene; absolute values of the nuclear co-ordinates as a function of time; measured slow-timescales associated with CH_2^+

References

(1) Zewail, A. H. Femtochemistry: atomic-scale dynamics of the chemical bond. *J. Phys. Chem. A* **2000**, 104, 5660.

(2) Lépine, F.; Ivanov, M.; Vrakking, M. J. J. Attosecond molecular dynamics: fact or fiction? *Nat. Photon.* **2014**, 8, 195.

(3) Nisoli, M.; Decleva, P.; Calegari, F.; Palacios, A.; Martín, F. Attosecond electron dynamics in molecules. *Chem. Rev.* **2017**, 117, 10760.

(4) Merritt, I. C. D.; Jacquemin, D.; Vacher, M. Attochemistry: Is Controlling Electrons the Future of Photochemistry? *J. Phys. Chem. Lett.* **2021**, 12, 8404.

(5) Sansone, G.; Kelkensberg, F.; Pérez-Torres, J. F.; Morales, F.; Kling, M. F.; Siu, W.; Ghafur, O.; Johnsson, P.; Swoboda, M.; Benedetti, E.; Ferrari, F.; Lépine, F.; Sanz-Vicario, J. L.; Zherebtsov, S.; Znakovskaya, I.; L'huillier, A.; Ivanov, M. Y.; Nisoli, M.; Martín, F.; Vrakking, M. J. J. Electron localization following attosecond molecular photoionization. *Nature* **2010**, 465, 763.

(6) Calegari, F.; Ayuso, D.; Trabattoni, A.; Belshaw, L.; De Camillis, S.; Anumula, S.; Frassetto, F.; Poletto, L.; Palacios, A.; Decleva, P.; Greenwood, J. B.; Martín, F.; Nisoli, M. Ultrafast electron dynamics in phenylalanine initiated by attosecond pulses. *Science* **2014**, 346, 336.

(7) Marciniak, A.; Despré, V.; Barillot, T.; Rouzée, A.; Galbraith, M. C. E.; Klein, J.; Yang, C.-H.; Smeenk, C.T.L.; Loriot, V.; Nagaprasad Reddy, S.; Tielens, A.G.G.M.; Mahapatra, S.; Kuleff, A. I.; Vrakking, M.J.J.; Lépine, F. XUV excitation followed by ultrafast non-adiabatic relaxation in PAH molecules as a femto-astrochemistry experiment. *Nat. Comm.* **2015**, 6, 7909.

(8) Hervé, M.; Despré, V.; Castellanos Nash, P.; Loriot, V.; Boyer, A.; Scognamiglio, A.; Karras, G.; Brédy, R.; Constant, E.; Tielens, A. G. G. M.; Kuleff, A. I.; Lépine, F. Ultrafast dynamics of correlation bands following XUV molecular photoionization. *Nat. Phys.* **2020**, 17, 327.

(9) Svoboda, V.; Michiels, R.; LaForge, A. C.; Med, J.; Stienkemeier, F.; Slavíček, P.; Wörner, H. J. Real-time observation of water radiolysis and hydrated electron formation induced by extreme-ultraviolet pulses. *Sci. Adv.* **2020**, 6, eaaz0385.

(10) Holland, D. M. P.; Shaw, D. A.; Hayes, M. A.; Shpinkova, L. G.; Rennie, E. E.; Karlssond, L.; Baltzer, P.; Wannberg, B. A photoabsorption, photodissociation and photoelectron spectroscopy study of C_2H_4 and C_2D_4. *Chem. Phys.* **1997**, 219, 91.

(11) Kosma, K.; Trushin, S. A.; Fuss, W.; Schmid, W. E.; Ultrafast dynamics and coherent oscillations in ethylene and ethylene-d_4 excited at 162 nm. *J. Phys. Chem. A* **2008**, 112, 7514.

(12) Tao, H.; Allison, T. K.; Wright, T. W.; Stooke, A. M.; Khurmi, C.; van Tilborg, J.; Liu, Y.; Falcone, R. W.; Belkacem, A.; Martinez, T. J. Ultrafast internal conversion in ethylene. I. The excited state lifetime. *J. Chem. Phys.* **2011** 134, 244306.

(13) Allison, T. K.; Tao, H.; Glover, W. J.; Wright, T. W.; Stooke, A. M.; Khurmi, C.; van Tilborg, J.; Liu, Y.; Falcone, R. W.; Martínez, T. J., Belkacem, A. Ultrafast internal conversion in ethylene. II. Mechanisms and pathways for quenching and hydrogen elimination. *J. Chem. Phys.* **2012**, 136, 124317.

(14) Kobayashi, T.; Horio, T.; Suzuki, T. Ultrafast deactivation of the $\pi\pi^*$(V) state of ethylene studied using sub-20 fs time-resolved photoelectron imaging. *J. Phys. Chem. A* **2015**, 119, 9518.

(15) van Tilborg, J.; Allison, T. K.; Wright, T. W.; Hertlein, M. P.; Falcone, R. W.; Liu, Y.; Merdji, H.; Belkacem, A. Femtosecond isomerization dynamics in the ethylene cation measured in an EUV-pump NIR-probe configuration. *J. Phys. B: At. Mol. Opt. Phys.* **2009**, 42, 081002.

(16) Ludwig, A.; Liberatore, E.; Herrmann, J.; Kasmi, L.; López-Tarifa, P.; Gallmann, L.; Rothlisberger, U.; Keller, U.; Lucchini, M. Ultrafast relaxation dynamics of the ethylene cation $C_2H_4^+$. *J. Phys. Chem. Lett.* **2016**, 7, 1901.

(17) Domcke, W.; Yarkony, D. R. Role of conical intersections in molecular spectroscopy and photoinduced chemical dynamics. *Annu. Rev. Phys. Chem.* **2012**, 63, 325.

(18) Boyer, A.; Hervé, M.; Despré, V.; Castellanos Nash, P.; Loriot, V.; Marciniak, A.; Tielens, A. G. G. M.; Kuleff, A. I.; Lépine, F. Ultrafast vibrational relaxation dynamics in XUV-excited polycyclic aromatic hydrocarbon molecules. *Phys. Rev. X* **2021**, 11, 041012.

(19) Bevington, P. R.; Robinson, D. K. Data Reduction and Error Analysis for the Physical Sciences. (McGraw-Hill Higher Education, New York, 2003).

(20) Roos, B. O.; Taylor, P. R.; Sigbahn, P. E. M.; A complete active space SCF method (CASSCF) using a density matrix formulated super-CI approach. *Chem. Phys.* **1980**, 48, 157.

(21) Roos, B. O.; Lindh, R.; Malmqvist, P.-A.; Veryazov, V.; Widmark, P.-O. Main group atoms and dimers studied with a new relativistic ANO basis set. *J. Phys. Chem. A* **2004**, 108, 2851.

(22) Aquilante, F.; Gagliardi, L.; Pedersen, T. B.; Lindh, R. Atomic Cholesky decompositions: a route to unbiased auxiliary basis sets for density fitting approximation with tunable accuracy and efficiency. *J. Chem. Phys.* **2009**, 130, 154107.

(23) Tully, J. C.; Preston, R. K. Trajectory surface hopping approach to non-adiabatic molecular collisions: The Reaction of H^+ with D_2. *J. Chem. Phys.* **1971**, 55, 562.

(24) Granucci, G.; Persico, M. Excited state dynamics with the direct trajectory surface hopping method: azobenzene and its derivatives as a case study. *Theo. Chem. Acc.* **2007**, 117, 1131.

(25) Galván, I. F. et al. OpenMolcas: From source code to insight. *J. Chem. Theory Comput.* **2019**, 15, 5925.

(26) Wigner, E. On the Quantum correction for thermodynamic equilibrium. *Phys. Rev.* **1932**, 40, 749.

(27) Barbatti, M.; Ruckenbauer, M.; Plasser, F.; Pittner, J.; Granucci, G.; Persico, M.; Lischka, H. Newton-X: a surface-hopping program for non-adiabatic molecular dynamics. *WIREs: Comput. Mol. Sci.* **2014**, 4, 26.

(28) Stockbauer, R.; Inghram, M. G. Threshold photoelectron-photoion coincidence mass spectrometric study of ethylene and ethylene-d_4. *J. Chem. Phys.* **1975**, 62, 4862.

(29) Joalland, B.; Mori, T.; Martínez, T. J.; Suits, A. G. Photochemical dynamics of ethylene cation $C_2H_4^+$. *J. Phys. Chem. Lett.* **2014**, 5, 1467.

(30) Gaire, B. et al. Photo-double-ionization of ethylene and acetylene near threshold. *Phys. Rev. A* **2014**, 89, 013403.

(31) Zinchenko, K. S.; Ardana-Lamas, F.; Seidu, I.; Neville, S. P.; van der Veen, J.; Lanfaloni, V. U.; Schuurman, M. S.; Wörner, H. J. Sub-7-femtosecond conical-intersection dynamics probed at the carbon K-edge. *Science* **2021**, 371, 489.

(32) Felkar, P. M.; Zewail, A. H. Rates of Photoisomerization of trans-stilbene in isolated and solvated Molecules: experiments on the deuterium isotope effect and RRKM Behavior. *J. Phys. Chem.* **1985**, 89, 5402.

(33) Delor, M.; Archer, S. A.; Keane, T.; Meijer, A. J. H. M.; Sazanovich, I. V.; Greetham, G. M.; Towrie, M.; Weinstein, J. A. Directing the path of light-induced electron transfer at a molecular fork using vibrational excitation. *Nat. Chem.* **2017**, 9, 1099.

(34) Schnedermann, C.; Yang, X.; Liebel, M.; Spillane, K. M.; Lugtenburg, J.; Fernández, I.; Valentini, A.; Schapiro, I.; Olivucci, M.; Kukura, P.; Mathies, R. A. Evidence for a vibrational phase-dependent isotope effect on the photochemistry of vision. *Nat. Chem.* **2018**, 10, 449.

(35) Ajay, J. S.; Komarova, K. G.; Remacle, F.; Levine, R. D. Time-dependent view of an isotope effect in electron-nuclear non-equilibrium dynamics with applications to N_2. *Proc. Natl. Acad. Sci. USA* **2018**, 115, 5890.

(36) Gonçalves, C.; Levine, R. D.; Remacle, F. Ultrafast geometrical reorganization of a methane cation upon sudden ionization: an isotope effect on electronic non-equilibrium quantum dynamics. *Phys. Chem. Chem. Phys.* **2021**, 23, 12051.

(37) Blavier, M.; Komarova, K.; Gonçalves, C. E. M.; Levine, R. D.; Remacle, F.. Electronic coherences steer the strong isotope effect in the ultrafast Jahn–Teller structural rearrangement of methane cation upon tunnel ionization. *J. Phys. Chem. A* **2021**, 125, 9495.

(38) Lee, J. W. L. et al. Time-resolved relaxation and fragmentation of polycyclic aromatic hydrocarbons investigated in the ultrafast XUV-IR regime. *Nat. Comm.* **2021**, 12, 6107.

(39) Barillot, T. et al. Correlation-driven transient hole dynamics resolved in space and time in the isopropanol molecule. *Phys. Rev. X* **2021**, 11, 031048.